Communication
doi.org/10.1002/chem.202000934

Polymeric Carbon Nitrides

Hydrazone-Linked Heptazine Polymeric Carbon Nitrides for Synergistic Visible-Light-Driven Catalysis

Wei Zhang,[a, b] Congying Xu,[a] Takeshi Kobayashi,[d] Yun Zhong,[a] Zhiyong Guo,*[a] Hongbing Zhan,[a] Marek Pruski,[c, d] and Wenyu Huang*[c, d]

Abstract: Heptazine-based conjugated polymeric carbon nitrides (PCNs) are promising metal-free photocatalysts, yet their synthesis is challenging due to the electron-deficiency and insolubility of heptazine units. Indeed, heptazine-containing polymers have only been prepared through nucleophilic substitution with amines by using toxic cyameluric chloride as the starting material. Herein, we report the novel and environmentally friendly method for preparing heptazine-based mesoporous PCNs with hydrazone links formed through a simple Schiff base condensation of melem-NH_2 and aldehydes. Unlike cyameluric chloride, melem-NH_2 is non-toxic, stable, and can be readily obtained from melem and hydrazine in solution. We demonstrate that the hydrazone linkages and the heptazine units synergistically enhance the photocatalytic activity of PCNs in visible-light-driven aerobic oxidation of benzyl alcohol to benzaldehyde. In particular, the polymer constructed from melem-NH_2 and *p*-phthalaldehyde shows 17 times more activity than graphitic carbon nitride (g-C_3N_4).

Visible-light-driven photocatalysis attracts increased attention because sunlight is a clean and renewable energy source and visible light accounts for 45% of the solar spectrum.[1] Polymeric carbon nitrides (PCNs) are of particular interest[2] as low-cost, non-toxic, metal-free polymeric semiconductors, which indeed have shown promising activity in visible light-driven photocatalytic reactions.[3] Chief among those is the family of graphitic carbon nitrides (g-C_3N_4), which can catalyze a variety of reactions, including water splitting, carbon dioxide conversion, oxidative coupling of amines, and degradation of rhodamine B.[4] The photocatalytic activity of g-C_3N_4 is attributed to the s-heptazine unit (melem, 2,5,8-triamino-tri-s-heptazine, see Scheme 1 a).[5] Typically, g-C_3N_4 is prepared by the pyrolysis of nitrogen-rich precursors including urea, thiourea, melamine, cyanamide, and dicyandiamide.[6] However, the catalytic efficiency of the resulting g-C_3N_4 is restricted by a low specific surface area and high electron–hole recombination rate.[7]

Numerous strategies have been reported to improve the surface area, dispersion, thermal/chemical stability, and chemical tunability of g-C_3N_4.[8] These include doping with hetero-

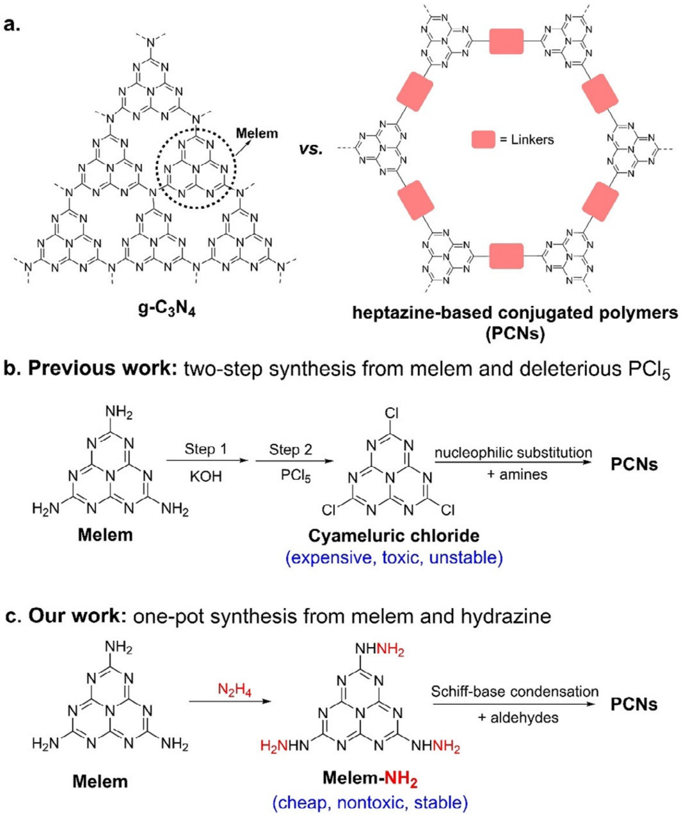

Scheme 1. a) The representative structures of g-C_3N_4 and heptazine-based PCNs. b) Previous and c) our strategies for the synthesis of PCNs by using two different heptazine precursors.

---

[a] W. Zhang, C. Xu, Y. Zhong, Prof. Z. Guo, Prof. H. Zhan
College of Materials Science and Engineering
Fuzhou University
Fuzhou 350108 (P. R. China)
E-mail: guozhy@fzu.edu.cn

[b] W. Zhang
Van't Hoff Institute for Molecular Sciences
University of Amsterdam
Science Park 904
1098 XH Amsterdam (The Netherlands)

[c] Prof. M. Pruski, W. Huang
Department of Chemistry
Iowa State University
Ames, IA 50011 (USA)
E-mail: whuang@iastate.edu

[d] T. Kobayashi, Prof. M. Pruski, W. Huang
Ames Laboratory, US Department of Energy
Ames, IA 50011 (USA)

Supporting information and the ORCID identification number(s) for the author(s) of this article can be found under:
https://doi.org/10.1002/chem.202000934.

atoms, nanocasting with hard templates, and introducing heterojunctions.[9] However, these top-down approaches are typically uncontrollable and time-consuming, giving low-quality g-C_3N_4 with low yields.[10]

The alternative, bottom-up, methods to synthesize PCNs from heptazine monomers offer better structural control but are challenged by the insolubility of most heptazine precursors in common organic solvents.[11] Moreover, the electron deficiency of heptazine rings hinders their reactivity.[12] Thus far, cyameluric chloride ($C_6N_7Cl_3$, also known as trichloroheptazine) is the only reactive heptazine precursor used for the preparation of heptazine-based PCNs.[13] Cyameluric chloride is typically synthesized from melem in two steps (Scheme 1 b), which use deleterious PCl_5 as the chlorinating reagent and release toxic $POCl_3$ as byproduct.[14] Therefore, developing heptazine precursors that are environmentally friendly and suitable for the facile design of versatile heptazine-based PCNs is highly desired.[15]

Here, we discovered a new, scalable, and environmentally friendly heptazine precursor, 2,5,8-trihydrazino-s-heptazine (melem-NH_2), which could react with aldehydes by a simple condensation to form heptazine-based PCNs connected through hydrazone linkages (Scheme 1 c and Figure 1 a). Melem-NH_2 is a non-toxic and stable compound that is readily prepared from melem and hydrazine in solution. Hydrazone, a trinuclear azomethine group (−N−N=C−), has been previously incorporated into covalent organic frameworks to improve their hydrolytic and oxidative stability as well as charge carrier mobility.[16] Particularly, we found *p*-phthalaldehyde to be the optimal aldehyde precursor that reacts with melem-NH_2 to yield a mesoporous organic polymer (MelonHP) featuring a high specific surface area, and thus more accessible active sites. Most importantly, the cross-linked hydrazone–heptazine repeating units in MelonHP synergistically enhanced its activity in the visible-light-driven oxidation of benzyl alcohol to benzaldehyde with O_2 under mild conditions. MelonHP showed a mass-specific activity enhancement factor of 17 compared to g-C_3N_4. To the best of our knowledge, this is the first report of synthesis and photocatalysis studies on such hydrazone–heptazine PCNs.

Figure 1 a briefly outlines the synthesis of hydrazone-linked heptazine PCNs by using 2,5,8-trihydrazino-s-heptazine (melem-NH_2) and aldehydes as starting materials through a Schiff base condensation reaction (see the Supporting Information for details). We initially chose *p*-phthalaldehyde, *m*-phthalaldehyde, and trimesaldehyde as the aldehyde precursors, and the resulting polymers are denoted as MelonHP, MelonHM, and MelonHT, respectively.

For all three polymers, the powder X-ray diffraction (PXRD) patterns did not show peaks from melem-NH_2; instead, a

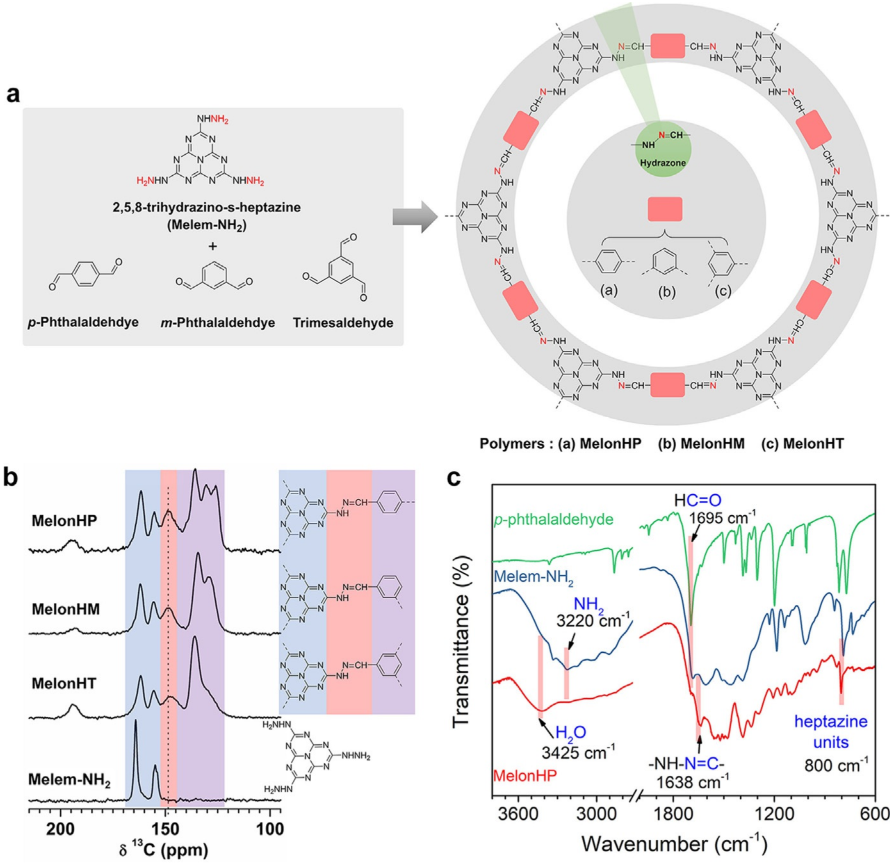

Figure 1. a) Schematic illustration of the synthesis of hydrazone-linked heptazine PCNs through melem-NH_2 condensation with different aldehydes. b) $^{13}C\{^1H\}$ CP MAS SSNMR spectra of MelonHP, MelonHM, and MelonHT (see the Supporting Information for NMR experimental details). c) FTIR spectra of MelonHP and the precursors (melem-NH_2 and *p*-phthalaldehyde).

broad peak was observed at $2\theta \approx 27°$ in line with (002) reflection of g-C_3N_4 (Figure S1 in the Supporting Information).[17] These observations suggest the formation of disordered heptazine networks with partly layered structures.[15] The transmission electron microscopy (TEM) images in Figure S2 show the representative morphology of MelonHP with the ultrathin and lamellar feature, upholding the XRD results.

We then studied the porous properties of the PCNs by using nitrogen adsorption–desorption measurements (Figure S3 and Table S1). Among all samples, only MelonHP showed a typical type-IV isotherm with a H4 hysteresis loop at relative pressures (P/P_0) from 0.7 to 0.9, indicating the presence of mesopores.[18] The specific Brunauer–Emmett–Teller (BET) surface area and pore volume were calculated to be $120\,m^2 g^{-1}$ and $0.44\,cm^3 g^{-1}$, respectively. By comparison, MelonHT gave a specific BET surface area of $25\,m^2 g^{-1}$, whereas MelonHM was nonporous. These results indicate that the type of aldehyde precursor plays a vital role in the pore formation of the hydrazine–heptazine-based organic network. Thermogravimetric analysis (TGA, Figure S4) under a N_2 flow showed the high thermal stability of MelonHP up to 350 °C. Additionally, the exact elemental compositions of these polymers were confirmed by X-ray photoelectron spectroscopy (XPS, see Figure S5).

The atomic-level structures of the three newly derived PCNs were examined by solid-state (SS) NMR and Fourier-transform infrared spectroscopy (Figures 1 b and c). The $^{13}C\{^1H\}$ cross-polarization magic-angle spinning (CPMAS) SSNMR spectra of MelonHP, MelonHM, and MelonHT displayed a distinct signal at $\delta = 150$ ppm, that can be assigned to the hydrazone carbon atom, –NHN=CH–.[19] The signals at $\delta = 120–140$ and 155–165 ppm were attributed to the carbon atoms in the phenyl and heptazine moieties, respectively. These assignments are in agreement with the resonances observed in a reference nonpolymeric compound MelonB, prepared through condensation reaction between melem-NH_2 and benzaldehyde (the synthesis details are given in the Supporting Information along with the NMR spectra, Figures S6 and S7), and with the results of a previous study.[20] To further confirm the formation of hydrazone linkages, we performed indirectly detected 2D $^1H\{^{15}N\}$ heteronuclear correlation (HETCOR) experiments (Figure 2),[21] which showed that cross peaks assigned to –*NH*–NH_2 and –NH–*NH_2* of melem-NH_2 disappeared after the reaction between melem-NH_2 and aldehydes. Instead, new signal appeared at $\delta_N \approx -220$ ppm and $\delta_H \approx 11$ ppm, which can be assigned to the hydrazone linkages –*NH*–N=CH– (note that non-protonated nitrogen was not observed due to the inefficient polarization transfer under the present experimental conditions).[22]

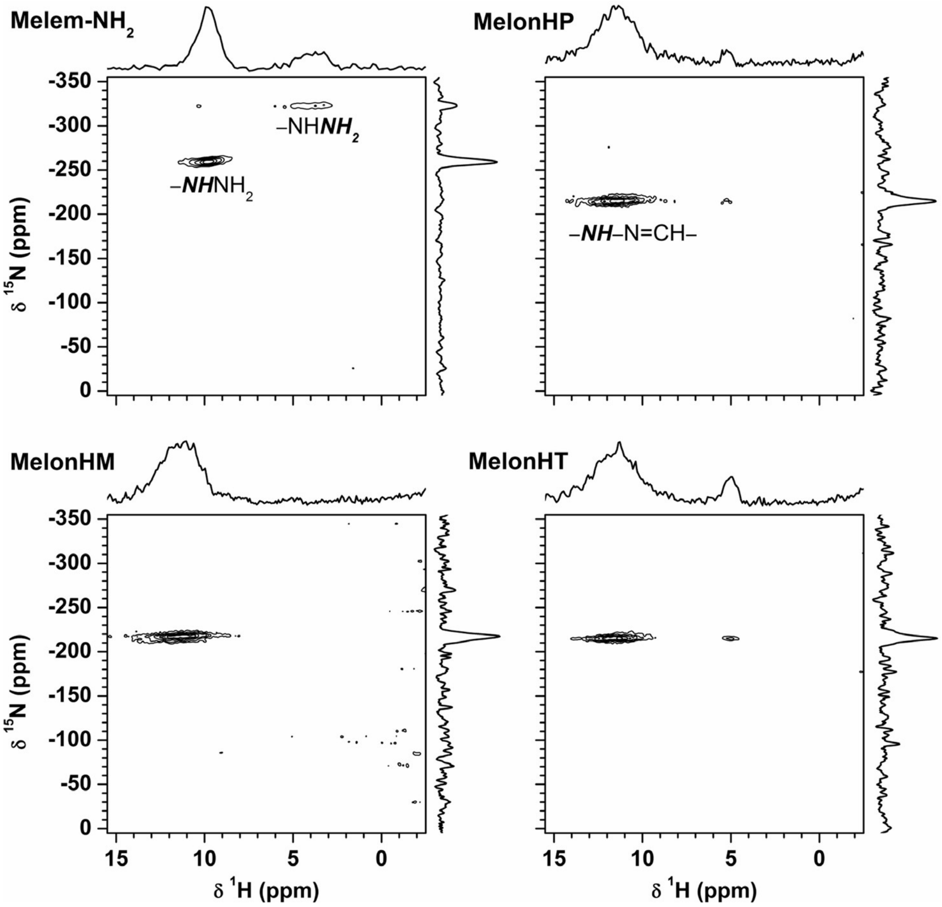

Figure 2. Indirectly-detected 2D $^1H\{^{15}N\}$ through-space HETCOR spectra of melem-NH_2 and derivative polymers. Experimental conditions are given in the Supporting Information.

The FTIR results are consistent with the SSNMR results. As shown in Figure 1 c, the MelonHP polymer combines the characteristic signals of the heptazine unit and the phenyl ring of its melem-NH_2 and *p*-phthalaldehyde precursors. Additionally, the FTIR spectra of MelonHP showed a vibration of the C=N bond at $\tilde{\nu} = 1554\,cm^{-1}$,[23] accompanied by the disappearance of the C=O stretching ($\tilde{\nu} = 1659\,cm^{-1}$, cf. *p*-phthalaldehyde) and amine signals ($\tilde{\nu} = 3220\,cm^{-1}$, cf. melem-$NH_2$).[24] This indicates the formation of hydrazone linkages (−NH−N=CH−) through condensation of the aldehyde and the amine.[25]

Taken together, the above SSNMR and FTIR results definitively show that all three samples consist of polymeric heptazine units cross-linked by hydrazone formed through condensation between melem-NH_2 and different aldehydes. The structural differences among MelonHP, MelonHM, and MelonHT derive from the locations of the formed imine bonds (or hydrazone) at either the *para* or *meta* position of the phenyl rings. The MelonHP shows the highest specific surface area, possibly due to a reduced steric hindrance between the melem units connected through the *para* sites of the aldehydes.

Notably, we were unable to prepare the PCNs by using the above-mentioned melem as precursor instead of melem-NH_2 (Scheme S1, see the Supporting Information).[26] Evidently, melem cannot react with aldehydes due to the electron-deficient heptazine ring that makes the $-NH_2$ groups inert to electrophilic attack.[13c] This was clearly confirmed by SSNMR spectroscopy; indeed, the only resonances observed in the $^{13}C\{^1H\}$ CP MAS spectrum of the melem-based product represented unreacted melem (Figure S8).

The MelonHM, MelonHT, and MelonHP polymers were then tested in the visible-light-driven oxidation of benzyl alcohols with O_2 (1 atm) to benzaldehyde, by using a 26 W white LED lamp as the light source (see the Supporting Information for details). As shown in Figure 3 a, control experiments confirmed that the reaction did not proceed in the absence of catalysts or without light, whereas g-C_3N_4 gave only 3% conversion. All three polymers proved to be active with >99% selectivity. MelonHP with the highest surface area exhibited the best photocatalytic performance among all catalysts tested in this study, giving a much higher conversion of 36% than MelonHM (3%), g-C_3N_4 (3%) and MelonHT (7%).

The mass-specific activities of these catalysts, calculated as millimole of benzaldehyde produced per gram of catalyst per hour under identical conditions, are shown in Figure 3 b. The catalytic performance in this series increased as follows: MelonHP $\gg$ MelonHT > MelonHM $\approx$ g-C_3N_4. Note that MelonHP outperformed g-C_3N_4 by a factor of 17, which indicates a strong synergistic effect between the hydrazone linkages and the heptazine units in MelonHP. The apparent quantum yield (AQY) of this light-driven process is consistent with the optical absorption (see the Supporting Information for details). In our case, the AQY was measured as a function of incident light wavelength by using bandpass filters with central wavelengths of 540 nm, which is close to the maximum absorbance of the melon-samples determined from the UV/Vis analysis (see below). MelonHP gave the highest AQY of 1.12%, showing a remarkably high activity for benzaldehyde production under this visible-light irradiation.

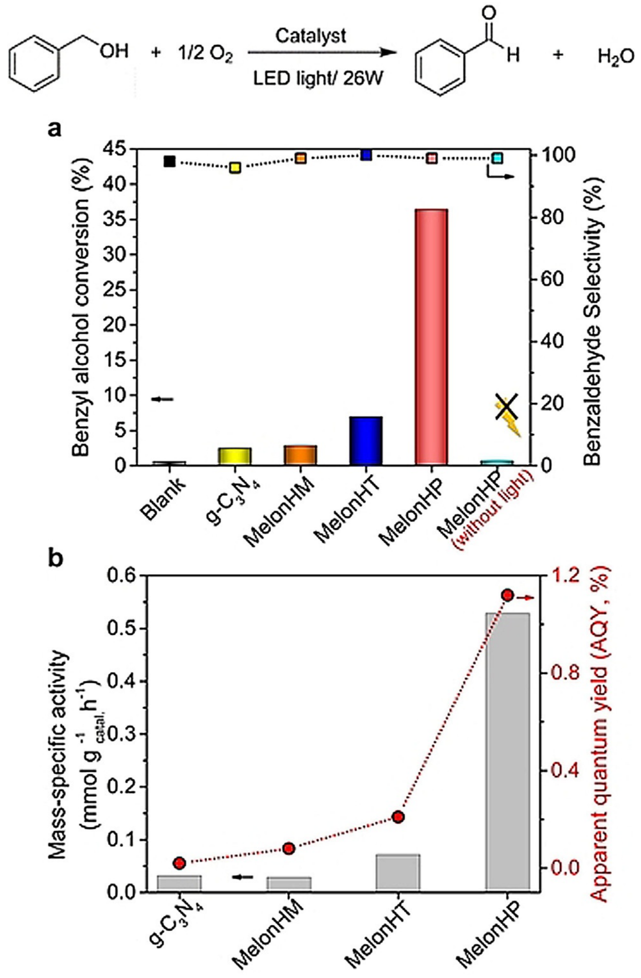

Figure 3. a) Comparisons of benzyl alcohol conversion and benzaldehyde selectivity over various photocatalysts for visible-light-induced photocatalytic aerobic oxidation to benzaldehyde. b) Mass-specific activity for the benzyl alcohol oxidation under visible-light irradiation calculated at <10% conversion; the apparent quantum yield (AQY) of these catalysts is measured at approximately 540 nm visible-light irradiation conditions.

To confirm the synergistic effect between the hydrazone linkages and the heptazine units in MelonHP on the photocatalytic oxidation, we prepared a previously reported heptazine-based porous polymer without hydrazone linkages by using cyameluric chloride and *p*-phenylenediamine as starting materials (Scheme S2).[13c] The resulting polymer, denoted as MelonP (Figure 4 a), was indeed hydrazone-free, as confirmed by SSNMR (Figure 4 b) and FTIR spectroscopy (Figure S9) (see the Supporting Information for details). The BET surface area of MelonP is $150\,m^2\,g^{-1}$ (Figure 4 c), which is higher than that of MelonHP ($120\,m^2\,g^{-1}$). For the latter, the hydrazone linkages in the heptazine-derived network lead to a flexible structure, and thus lower crystallinity and porosity.[27] Intriguingly, in spite of a higher surface area, MelonP gave much lower benzaldehyde conversion (14%) than MelonHP (36%). Figure 4 d shows that the area-specific activity for MelonHP is four times higher than that of MelonP. The higher activity of MelonHP over MelonP

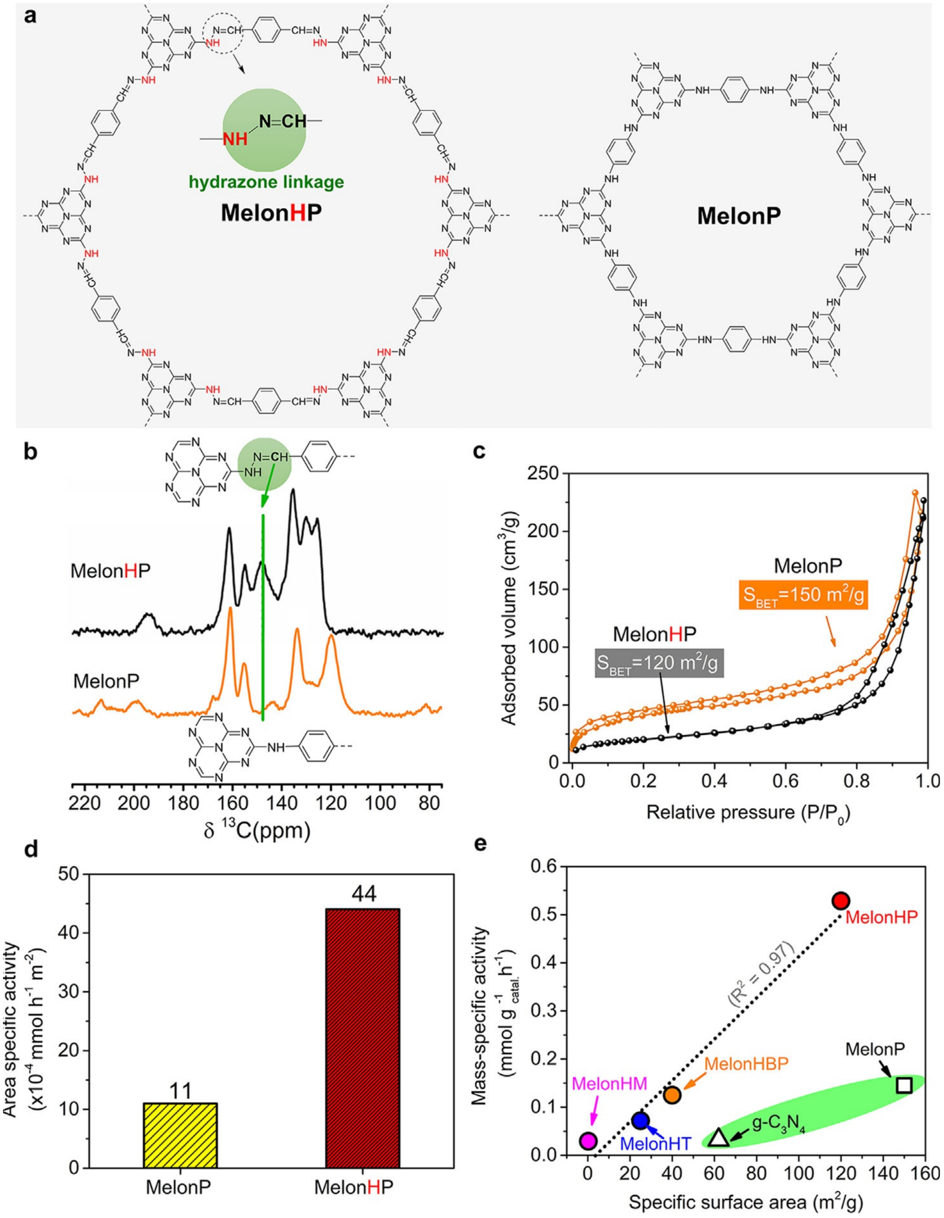

Figure 4. a) Schematic illustration of two heptazine-based PCNs: MelonHP and Hydrazone-free MelonP. b) $^{13}C\{^{1}H\}$ CP MAS SSNMR spectra and c) nitrogen adsorption–desorption isotherms of MelonP and MelonHP. d) Comparisons of the area-specific activity of MelonP and MelonHP. e) Plot for the correlation between the mass-specific activity of benzyl alcohol oxidation on hydrazine catalysts and their specific surface area, compared with porous g-C_3N_4 and MelonP.

supports the synergistic effect between the hydrazone linkages and the heptazine units in MelonHP.

Based on the above results, it is reasonable to expect that the catalytic performance of hydrazone-linked PCNs correlates well with the amount of exposed hydrazine–heptazine pairs. To substantiate this inference, we plotted, in Figure 4e, the mass-specific activities of the studied polymers (MelonHM, MelonHT, MelonHP, MelonP, and g-C_3N_4) against their BET surface areas. Indeed, the activities of hydrazone-linked PCNs show a strong linear correlation with their specific surface areas ($R^2 = 0.97$), which corroborates the synergistic effect between hydrazone and the heptazine units. Notably, g-C_3N_4 and MelonP, which do not feature the hydrazone linkages, are two exceptions with relatively high surface area (see Table S1) but low activity.

Inspired by this finding, we explored the possibility to further increase the catalytic activity by preparing materials with higher surface areas than MelonHP. First, we synthesized another PCN catalyst with hydrazone–heptazine sites, denoted as MelonHBP (see Scheme S3 and Figure S10) by using a larger dialdehyde precursor molecule (4,4′-biphenyldicarboxaldehyde). Although the resulting product had a surface area of only 40 $m^2 g^{-1}$, its catalytic activity followed exactly the trend discussed above (see Figure 4e). Secondly, we attempted the preparation of high-surface-area covalent organic frameworks (COFs) composed of hydrazone linkages. However, we tested various synthesis conditions and found that we could not obtain hydrazone-linked COFs, possibly due to the flexible hydrazone linkage with a sp^3 N atom.

The synergistic effect between the hydrazone linkages and heptazine units was further explored by UV/Vis diffuse reflectance spectroscopy (UV/Vis DRS) and density functional theory (DFT) calculations. As shown in Figure S11, the hydrazone-free MelonP exhibited an absorption edge at approximately 550 nm in the visible-light region (>400 nm). Upon introducing hydrazone to the heptazine-derived network, the absorption band became red-shifted to about 700 nm for MelonHP, MelonHM, and MelonHT. This indicates that the hydrazone moiety can significantly enhance visible light absorption of the PCNs. We calculated the band gap energy (E_g) by the plot of $[F(R_\infty)h\nu]^{1/2}$ versus $h\nu$, where $F(R_\infty)$ is the Kubelka–Munk function and $h\nu$ is the photon energy (Figure S12). All of the hydrazine polymers showed a narrower band gap (2.4–2.5 eV) than MelonP (3.58 eV, see Figure S12, inset). This is probably due to the strong electron-donating effect caused by the lone pair of electrons on the hydrazone group, reducing the band gap of the heptazine-based PCNs.[28]

By using DFT with the CP2K software package,[29] we studied the theoretical highest occupied molecular orbital (HOMO) and the lowest unoccupied molecular orbital (LUMO) energy levels of these PCNs. Figure S13 showed that the HOMO of representative MelonP models is localized in the heptazine unit. For MelonHP, however, the corresponding electron density is shifted to the hydrazone moiety with a higher HOMO by 0.4 eV in comparison to that of MelonP (Figure S14). The calculated band gap of MelonHP is narrower (2.9 eV) than that of MelonP (3.8 eV), which agrees well with the UV/Vis DRS results. Therefore, the introduction of hydrazone linkages can enhance the visible-light absorption and charge separation efficiency in MelonHP for the photocatalytic oxidation of benzyl alcohol (Scheme 2). Further experiments are needed to elucidate the active oxidative species that are responsible for this photocatalytic oxidation reaction.

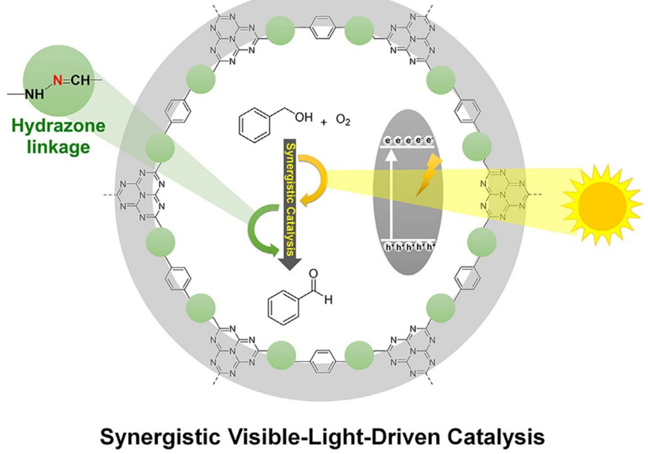

Scheme 2. Synergistic effect of hydrazone linkages in visible-light-driven aerobic oxidation of benzyl alcohol to benzaldehyde over hydrazone-inked heptazine-based mesoporous polymer.

In conclusion, we have developed a facile method to synthesize a series of new heptazine-based PCNs with hydrazone linkage through the condensation of melem-NH_2 and different aldehydes. Our results identified *p*-phthalaldehyde as the optimal aldehyde precursor, giving a robust mesoporous polymer (MelonHP) with highly cross-linked hydrazone–heptazine repeating units. The synthesized MelonHP showed high efficiency as a catalyst for visible-light-driven oxidation of benzyl alcohol to benzaldehyde with oxygen under mild conditions. Control experiments and DFT calculations showed that the hydrazone linkages in the PCNs play a vital role in this photocatalytic reaction, making MelonHP 17 times more active than g-C_3N_4. This synergistic effect between hydrazone linkages and heptazine units is further confirmed by the much lower photocatalytic activity of an analogous heptazine-based porous polymer without the hydrazone moiety (MelonP). This work provides a new approach for designing highly efficient metal-free catalysts for photocatalytic aerobic oxidation of alcohols under visible light.

Acknowledgements

This work was supported by the financial support from the National Natural Science Foundation of China (Grant No. 51703031). W.Z. thanks the China Scholarship Council for a Ph.D. fellowship (201506140058). T.K. and M.P. (SSNMR) are supported by the U.S. Department of Energy (DOE), Office of Science, Basic Energy Sciences, Division of Chemical Sciences, Geosciences, and Biosciences. Ames Laboratory is operated for the DOE by Iowa State University under Contract No. DE-AC02-07CH11358. We also acknowledge the support from Iowa Energy Center and Iowa State University.

Conflict of interest

The authors declare no conflict of interest.

Keywords: heptazines · hydrazone linkages · porous polymers · synergistic effects · visible light

[1] J. C. Colmenares, R. Luque, *Chem. Soc. Rev.* **2014**, *43*, 765–778.
[2] X. Wang, K. Maeda, A. Thomas, K. Takanabe, G. Xin, J. M. Carlsson, K. Domen, M. Antonietti, *Nat. Mater.* **2008**, *7*, 76.
[3] a) W.-J. Ong, L.-L. Tan, Y. H. Ng, S.-T. Yong, S.-P. Chai, *Chem. Rev.* **2016**, *116*, 7159–7329; b) S. Xu, P. Zhou, Z. Zhang, C. Yang, B. Zhang, K. Deng, S. Bottle, H. Zhu, *J. Am. Chem. Soc.* **2017**, *139*, 14775–14782.
[4] a) Y. Wang, X. Wang, M. Antonietti, *Angew. Chem. Int. Ed.* **2012**, *51*, 68–89; *Angew. Chem.* **2012**, *124*, 70–92; b) F. Su, S. C. Mathew, G. Lipner, X. Fu, M. Antonietti, S. Blechert, X. Wang, *J. Am. Chem. Soc.* **2010**, *132*, 16299–16301; c) Y. Xiao, G. Tian, W. Li, Y. Xie, B. Jiang, C. Tian, D. Zhao, H. Fu, *J. Am. Chem. Soc.* **2019**, *141*, 2508–2515.
[5] a) Y. Zheng, Y. Jiao, Y. Zhu, L. H. Li, Y. Han, Y. Chen, A. Du, M. Jaroniec, S. Z. Qiao, *Nat. Commun.* **2014**, *5*, 3783; b) Y. Zheng, Y. Jiao, Y. Zhu, Q. Cai, A. Vasileff, L. H. Li, Y. Han, Y. Chen, S.-Z. Qiao, *J. Am. Chem. Soc.* **2017**, *139*, 3336–3339.
[6] Y. Dong, Q. Wang, H. Wu, Y. Chen, C.-H. Lu, Y. Chi, H.-H. Yang, *Small* **2016**, *12*, 5376–5393.
[7] G. Marcì, E. I. García-López, L. Palmisano, *Catal. Today* **2018**, *315*, 126–137.

[8] a) J. Pan, L. Guo, S. Zhang, N. Wang, S. Jin, B. Tan, *Chem. Asian J.* **2018**, *13*, 1674 – 1677; b) W. Zhang, T. Liu, H. Wu, P. Wu, M. He, *Chem. Commun.* **2015**, *51*, 682 – 684.

[9] a) A. Savateev, M. Antonietti, I. Ghosh, B. König, *Angew. Chem. Int. Ed.* **2018**, *57*, 15936 – 15947; *Angew. Chem.* **2018**, *130*, 16164 – 16176; b) G. Zhang, Z.-A. Lan, X. Wang, *Chem. Sci.* **2017**, *8*, 5261 – 5274; c) G. Peng, L. Xing, J. Barrio, M. Volokh, M. Shalom, *Angew. Chem. Int. Ed.* **2018**, *57*, 1186 – 1192; *Angew. Chem.* **2018**, *130*, 1200 – 1206; d) M. Zhu, S. Kim, L. Mao, M. Fujitsuka, J. Zhang, X. Wang, T. Majima, *J. Am. Chem. Soc.* **2017**, *139*, 13234 – 13242.

[10] Y. Zheng, L. Lin, B. Wang, X. Wang, *Angew. Chem. Int. Ed.* **2015**, *54*, 12868 – 12884; *Angew. Chem.* **2015**, *127*, 13060 – 13077.

[11] L. Maxwell, S. Gómez-Coca, T. Weyhermüller, D. Panyella, E. Ruiz, *Dalton Trans.* **2015**, *44*, 15761 – 15763.

[12] S. Kumar, N. Sharma, K. Kailasam, *J. Mater. Chem. A* **2018**, *6*, 21719 – 21728.

[13] a) K. Kailasam, J. Schmidt, H. Bildirir, G. Zhang, S. Blechert, X. Wang, A. Thomas, *Macromol. Rapid Commun.* **2013**, *34*, 1008 – 1013; b) Q.-Q. Dang, Y.-F. Zhan, X.-M. Wang, X.-M. Zhang, *ACS Appl. Mater. Interfaces* **2015**, *7*, 28452 – 28458; c) K. Kailasam, M. B. Mesch, L. Möhlmann, M. Baar, S. Blechert, M. Schwarze, M. Schröder, R. Schomäcker, J. Senker, A. Thomas, *Energy Technol.* **2016**, *4*, 744 – 750.

[14] A. Schwarzer, T. Saplinova, E. Kroke, *Coord. Chem. Rev.* **2013**, *257*, 2032 – 2062.

[15] P. Kumar, E. Vahidzadeh, U. K. Thakur, P. Kar, K. M. Alam, A. Goswami, N. Mahdi, K. Cui, G. M. Bernard, V. K. Michaelis, K. Shankar, *J. Am. Chem. Soc.* **2019**, *141*, 5415 – 5436.

[16] a) L. Shen, N. Cao, L. Tong, X. Zhang, G. Wu, T. Jiao, Q. Yin, *y. Pan, H. Li, Angew. Chem. Int. Ed.* **2018**, *57*, 16486 – 16490; *Angew. Chem.* **2018**, *130*, 16724 – 16728; b) D. N. Bunck, W. R. Dichtel, *J. Am. Chem. Soc.* **2013**, *135*, 14952 – 14955; c) P. Data, P. Pander, P. Zassowski, V. Mimaite, K. Karon, M. Lapkowski, J. V. Grazulevicius, P. Slepski, K. Darowicki, *Electrochim. Acta* **2017**, *230*, 10 – 21; d) H. K. Singh, B. Pradhan, S. K. Singh, R. Nandi, D. S. S. Rao, S. K. Prasad, A. S. Achalkumar, B. Singh, *ChemistrySelect* **2018**, *3*, 4027 – 4037.

[17] G. Zhang, G. Li, T. Heil, S. Zafeiratos, A. Savateev, X. Wang, M. Antonietti, *Angew. Chem. Int. Ed.* **2019**, *58*, 3433 – 3437; *Angew. Chem.* **2019**, *131*, 3471 – 3475.

[18] C. Gao, G. Chen, X. Wang, J. Li, Y. Zhou, J. Wang, *Chem. Commun.* **2015**, *51*, 4969 – 4972.

[19] F. J. Uribe-Romo, C. J. Doonan, H. Furukawa, K. Oisaki, O. M. Yaghi, *J. Am. Chem. Soc.* **2011**, *133*, 11478 – 11481.

[20] B. V. Lotsch, M. Döblinger, J. Sehnert, L. Seyfarth, J. Senker, O. Oeckler, W. Schnick, *Chem. Eur. J.* **2007**, *13*, 4969 – 4980.

[21] a) T. Kobayashi, Y. Nishiyama, M. Pruski in *Modern Methods in Solid-state NMR: A Practitioner's Guide*, RSC, London, **2018**, pp. 1 – 38; b) W. Wiench, C. E. Bronnimann, V. S.-Y. Lin, M. Pruski, *J. Am. Chem. Soc.* **2007**, *129*, 12076 – 12077.

[22] P. Šimůnek, V. Bertolasi, A. Lyčka, V. Macháček, *Org. Biomol. Chem.* **2003**, *1*, 3250 – 3256.

[23] a) L. Zou, X. Yang, S. Yuan, H.-C. Zhou, *CrystEngComm* **2017**, *19*, 4868 – 4871; b) Z.-J. Li, S.-Y. Ding, H.-D. Xue, W. Cao, W. Wang, *Chem. Commun.* **2016**, *52*, 7217 – 7220.

[24] a) C. R. DeBlase, K. E. Silberstein, T.-T. Truong, H. D. Abruña, W. R. Dichtel, *J. Am. Chem. Soc.* **2013**, *135*, 16821 – 16824; b) L. Lin, H. Guan, D. Zou, Z. Dong, Z. Liu, F. Xu, Z. Xie, Y. Li, *RSC Adv.* **2017**, *7*, 54407 – 54415.

[25] L. Stegbauer, K. Schwinghammer, B. V. Lotsch, *Chem. Sci.* **2014**, *5*, 2789 – 2793.

[26] T.-O. Do, *ChemSusChem* **2019**, *12*, 291 – 302.

[27] T. Kundu, J. Wang, Y. Cheng, Y. Du, Y. Qian, G. Liu, D. Zhao, *Dalton Trans.* **2018**, *47*, 13824 – 13829.

[28] T. W. Goh, C. Xiao, R. V. Maligal-Ganesh, X. Li, W. Huang, *Chem. Eng. Sci.* **2015**, *124*, 45 – 51.

[29] J. Hutter, M. Iannuzzi, F. Schiffmann, J. VandeVondele, *Wiley Interdiscip. Rev.: Comput. Mol. Sci.* **2014**, *4*, 15 – 25.

Manuscript received: February 20, 2020
Accepted manuscript online: February 23, 2020
Version of record online: June 2, 2020

Chemistry–A European Journal

Supporting Information

Hydrazone-Linked Heptazine Polymeric Carbon Nitrides for Synergistic Visible-Light-Driven Catalysis

Wei Zhang,[a, b] Congying Xu,[a] Takeshi Kobayashi,[d] Yun Zhong,[a] Zhiyong Guo,*[a]
Hongbing Zhan,[a] Marek Pruski,[c, d] and Wenyu Huang*[c, d]

Experimental Section

Materials and instrumentation

Starting materials and solvents were purchased and used without further purification from commercial suppliers (Sigma-Aldrich, Alfa Aesar and TCI). Melem was synthesized by a literature method. [1] The PXRD data were collected on a Rigaku Ultima III X-ray diffractometer using Cu-Kα radiation at 35 kV and 30 mA. UV-Vis diffuse reflectance spectra were recorded on PE Lambda 950 UV-Vis spectrophotometer. Pore volume and surface area measurements using high purity nitrogen were performed using Micromeritics ASAP 2020 plus gas sorption analyzer at 77 K. The specific surface area was calculated according to Brunauer–Emmett–Teller (BET) theory in the relative pressure range P/P_0 = 0.05–0.30. Transmission electron microscopy (TEM) micrographs were measured on FEI Tecnai-G^2-F20 transmission electronic microscope. The Fourier Transform Infrared (FTIR) spectra were measured on a Thermo Fisher Scientific Nicolet 5700 FTIR spectrometer. The C, H and N contents of the polymer were measured using an elemental analyzer (Vario EL Cube). The X-ray photoelectron spectra (XPS) measurements were performed using a PHI 5500 Multi-technique system (Physical Electronics, Chanhassen, MN) with a monochromatized Al Kα X-ray source (hv = 1486.6 eV). The data were collected on the dried and powdered samples. The sample is pressed onto an indium substrate and is fixed on a sample holder. High-resolution C1s, O1s, and N1s peaks were collected and then fitted using CasaXPS software (RBD Instruments, Bend, OR).

Solid-State NMR spectroscopy.

The spectra of naturally ^{13}C and ^{15}N-abundant melem-NH$_2$, MelonHP, MelonHM, and MelonHT were acquired at 14.1 T, on a Varian NMR system spectrometer using a 1.6-mm FastMAS® probe. The samples were packed in magic-angle spinning (MAS) zirconia rotors in an ambient atmosphere. The ^{13}C spectra were acquired by means of one-dimensional (1D) $^{1}\text{H}\rightarrow{}^{13}\text{C}$ cross-polarization under MAS (CPMAS). In the case of ^{15}N, 2D ^{1}H-^{15}N heteronuclear correlation (HETCOR) spectra were acquired, using the so-called indirect detection for improved sensitivity.[2-3] The experimental parameters are listed below, where ν_R is the MAS rate, $\nu_{RF}(X)$ is the magnitude of the RF magnetic field applied to X spins, τ_{CP} is the CP time, Δt_1 is the increment of t_1 during 2D acquisition, NS is the number of scans, τ_{RD} is the recycle delay, and AT is the acquisition time.

^{13}C{^{1}H} CPMAS: ν_R = 40 kHz, $\nu_{RF}(^{1}\text{H})$ during 90° pulse = 125 kHz, $\nu_{RF}(^{1}\text{H})$ during CP = 60 kHz, $\nu_{RF}(^{1}\text{H})$ during heteronuclear SPINAL64 decoupling = 10 kHz, $\nu_{RF}(^{13}\text{C})$ during CP = 100 kHz, τ_{CP} = 1.5 ms, NS = 1600, τ_{RD} = 1 s, and AT = 27 min.

^{1}H{^{15}N} HETCOR: ν_R = 40 kHz, $\nu_{RF}(^{1}\text{H})$ during 90° pulse = 125 kHz, $\nu_{RF}(^{1}\text{H})$ during CP = 60 kHz, $\nu_{RF}(^{1}\text{H})$ during HORROR recoupling = 20 kHz, $\nu_{RF}(^{1}\text{H})$ during heteronuclear SPINAL64 decoupling = 10 kHz, $\nu_{RF}(^{15}\text{N})$ during CP and 90° pulses = 100 kHz, $\nu_{RF}(^{15}\text{N})$ during heteronuclear SPINAL64 decoupling = 10 kHz, τ_{CP} during $^{1}\text{H}\rightarrow{}^{15}\text{N}$ and $^{15}\text{N}\rightarrow{}^{1}\text{H}$ CP transfers = 2.0 ms, Δt_1 = 25 μs, 256 rows with NS per row = 80 (States-TPPI), τ_{RD} = 1 s, and AT = 11.8 h.

The chemical shifts are referenced to TMS (δ_H and δ_C) and nitromethane (δ_N) at 0 ppm.

Procedure for melon-related polymer preparation

Synthesis of Melem-NH$_2$

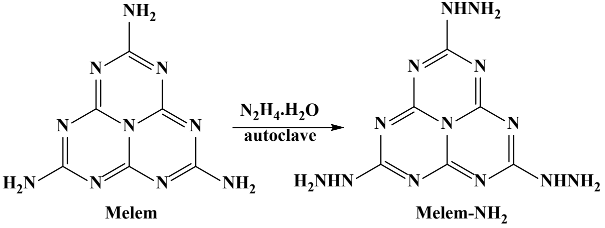

20 mL 80% Hydrazine solution in water and 3.2 g melem were mixed in a 100 mL Teflon lined autoclave. The tightly closed set-up was placed in a drying oven and heated up to 140 °C. After 24 h at this temperature, the autoclave was cooled down to room temperature and the obtained yellow suspension was placed in a 100 mL beaker. To this suspension, a 10 % solution of HCl was added until the pH of the solution was between 1 and 2. By the following filtration of the mixture, the unreacted solid residue was separated and the filtrate was treated with 10 % NaOH solution. The product was precipitated at a pH value of the solution of 7.5–8.5 and washed with excessive water. The obtained solid was dissolved in 10 % HCl again (pH = 1), filtered off once more, and precipitated with NaOH solution (pH = 8). This procedure was repeated three times, and then the resulting yellow solid was washed with methanol and dried under vacuum. ^{13}C NMR and IR data were in good agreement with the reported values.

Synthesis of Cyameluric chloride

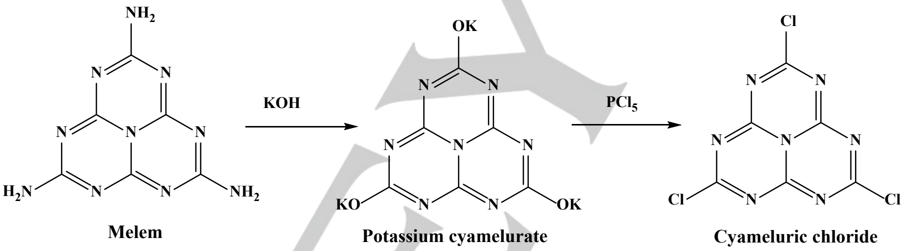

A mass of 2.5 g (12 mmol) purified melem powder was placed in a 100 mL round-bottomed Schlenk flask. A solution of 2.5 M KOH(aq) was added to the flask to a total volume of 25 mL. The stirred mixture was then heated to reflux (≈160 °C) in air with an oil bath for 6 hrs. The resulting clear, dark orange solution was cooled naturally to room temperature, overnight. Long, colorless, needle-like crystals grew from this solution and were separated by filtration via Buchner funnel, rinsed with ethanol, and then acetone. The product was dried at 100 °C under vacuum (0.78 g, yield 20 %). A glass tube (o.d. × i.d. = 10 × 8 mm^2) was charged with anhydrous $C_6N_7(OK)_3$ (84 mg) and PCl_5 (178 mg), flame-sealed under vacuum. The reaction mixture was heated at 100 °C for 7 h and 140 °C for 24 h to afford a yellow solid. The product was removed from the glass tube and slowly poured into ice water with stirring. The undissolved $C_6N_7Cl_3$ was filtered by suction, dried at 80 °C under dynamic vacuum. The product (40 mg, yield 64%) was used at the next step immediately. FT-IR (KBr, cm^{-1}): 646 (m), 825 (s), 942 (s), 1087 (m), 1200 (s), 1307 (s), 1500 (s), 1650 (s).

Synthesis of MelonHP

A flame dried Schlenk flask fitted with a condenser and a magnetic stirring bar was charged with Melem-NH_2 (489 mg, 1.86 mmol), terephthalaldehyde (450 mg, 3.35 mmol) and DMSO (32 mL). After degassing by argon bubbling the mixture was heated to 120 °C for 120 h under an inert atmosphere. After it was cooled down to room temperature, the precipitates were collected by filtration and washed with excess DMSO, acetone, and THF respectively. Finally, the product was extracted with THF in a Soxhlet apparatus for 2 days and dried at 100 °C under vacuum to give a yellow solid in 61 % yield.

Synthesis of MelonHM

In a fashion similar to the preparation of melonHP, Melem-NH_2 (489 mg, 1.86 mmol) and isophthalaldehyde (450 mg, 3.35 mmol) were reacted in 36 mL DMSO at 120 °C for 120 h to afford MelonHM in 53% yield.

Synthesis of MelonHT

In a fashion similar to the preparation of melonHP, Melem-NH_2 (326 mg, 1.24 mmol) and 1,3,5-Benzenetricarboxaldehyde (228 mg, 1.40 mmol) were reacted in 40 mL DMSO at 120 °C for 120 h to afford MelonHT in 58% yield.

Synthesis of MelonP

A flame dried Schlenk flask fitted with a condenser and a magnetic stirring bar was charged with cyameluric chloride (103.8 mg, 0.38 mmol) and 15 mL anhydrous tetrahydrofuran (THF). Then the solution of *p*-phenylenediamine (31.5 mg, 0.28 mmol) in 10 mL THF was added to the above solution dropwise. The solution is stirred at -10°C under nitrogen atmosphere and after 3 h, Na_2CO_3 was added to neutralize HCl, which is formed during the reaction. Subsequently, the yellow reaction mixture was poured into ice-cold water, the precipitate was filtered and washed successively with cold water, THF, and $CHCl_3$ and dried under vacuum to give a yellow solid in 64 % yield.

Catalytic performance test

The reaction was carried out in a sealed 6-dram glass vial (22.2 mL) with a magnetic stirrer. In a typical reaction, 10 mg catalyst was evacuated at 100 °C under vacuum to remove any absorbed species. The vial was then saturated with O_2 and 3 mL toluene was injected into the vial. The suspension was sonicated for 5 mins, to disperse the catalyst homogeneously. Mesitylene (10 µL, 0.07 mmol), and benzyl alcohol (25.0 µL, 0.24 mmol) were injected into the reaction vial. The suspension was stirred for 30 mins in the dark to achieve equilibrium. An O_2 balloon was used to ensure the atmospheric O_2 pressure was maintained at 0.1 MPa. The reaction vial was then placed in a 100 °C oil bath and irradiated with a 26 W Helical bulb for 24 hours.

The apparent quantum efficiency (Φ_{AQE}) was calculated by the following equation:

$$\Phi_{AQE} = N_{reacted}/N_{incident} = (2 \times n_{mol} \times N_A \times h \times c)/(I \times S \times \lambda \times t)$$

$$N_{incident} = (I \times S \times \lambda \times t)/(h \times c) \qquad N_{reacted} = 2 \times n_{mol} \times N_A$$

In the equation above, t is the time (1 h = 3600 s), h is Planck's constant, and c is the speed of light in free space.

n_{mol} = the molar quantities of product; I is the light power density

$N_A = 6.02\times10^{23}$ mol^{-1}; $S = 2.52$ cm^2; $c = 3\times10^8$ m/s; $\lambda = 540$ nm $= 5.4\times10^{-7}$ m; $h = 6.62\times10^{-34}$ J·S

DFT calculation

DFT calculations were performed using the CP2K software package,[4] using the combined Gaussian and plane-wave (GPW) method for the calculation of energies.[5] The BLYP functional was used for the exchange-correlation.[6] The valence orbitals were described by DZVP-GTH Gaussian basis set, all calculations were carried out using the PBE density functional augmented with the Grimme D3 dispersion correction. The plane wave kinetic energy cut-off was set to 400 eV. Visualization of the geometrical structures and electrostatic potential mapped onto electron density surfaces were performed by Avogadro software.

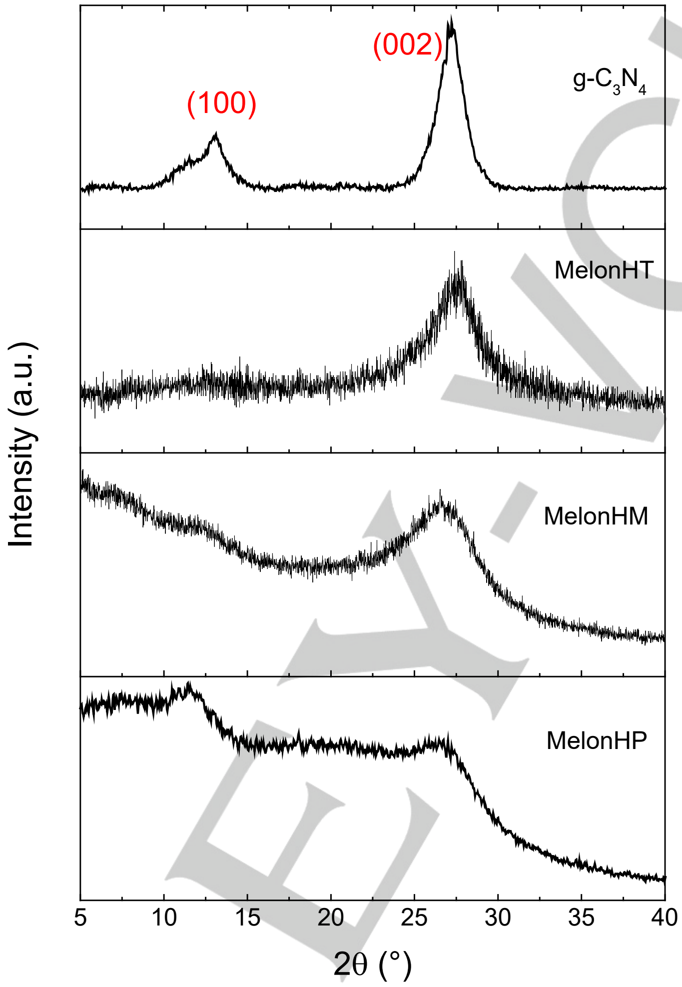

Figure S1 X-ray diffraction patterns of MelonHP, MelonHM, MelonHT and g-C_3N_4.

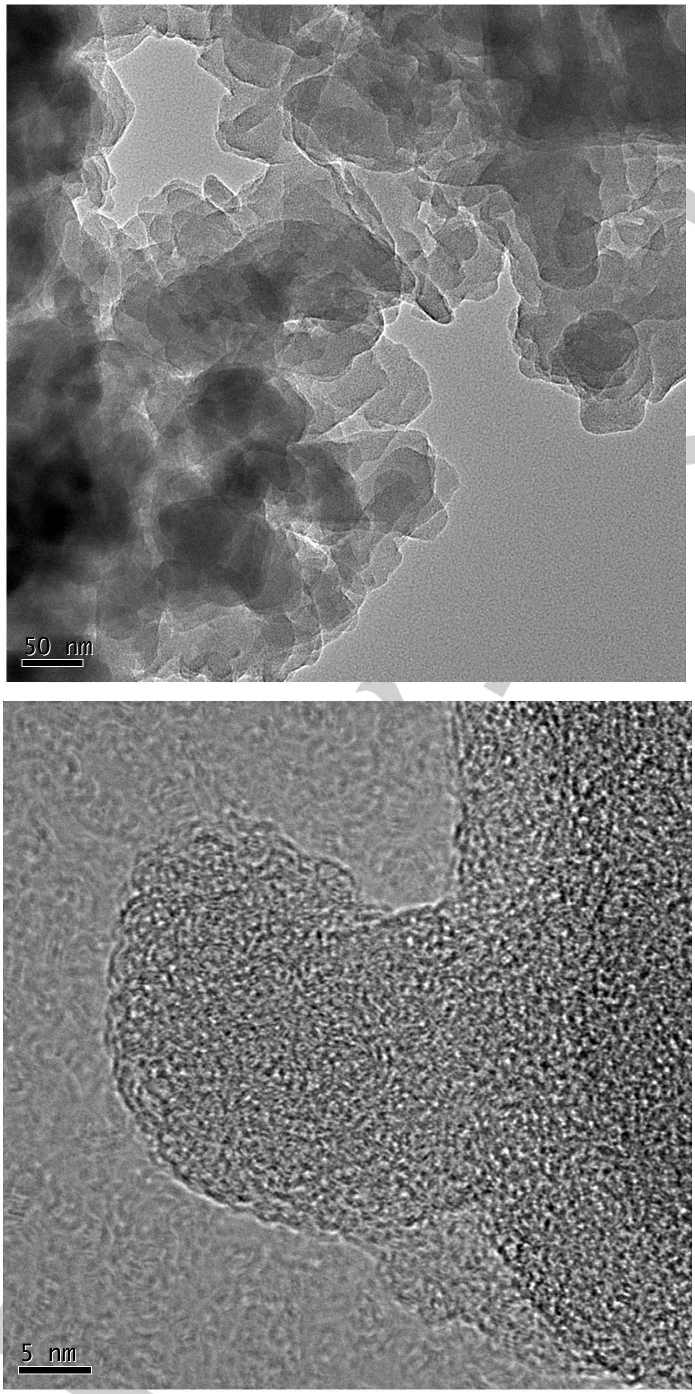

Figure S2. Representative TEM images of MelonHP.

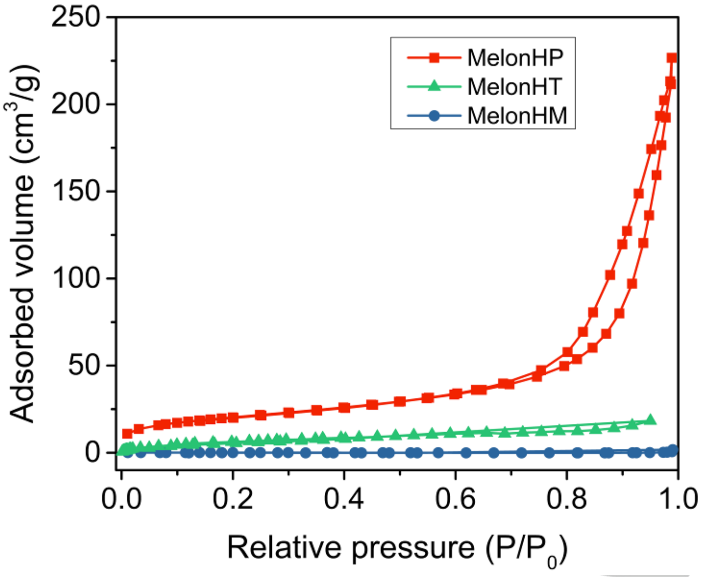

Figure S3 Nitrogen adsorption-desorption isotherms of MelonHP, MelonHM and MelonHP.

Table S1 Textural properties of the MelonHP, MelonHM and MelonHT samples.

Entry	Sample	S_{BET} (m^2/g) [a]	V_{total} (cm^3/g) [a]	C (wt. %) [b]	N (wt. %) [b]
1	MelonHP	120	0.44	33.6	42.3
2	MelonHM	0.26	-	34.1	46.1
3	MelonHT	25	0.03	32.6	39.4
4	MelonP	150	0.41	36.9	31.2
5[c]	g-C_3N_4	62	0.32	-	-

[a] Calculated (based on N_2 sorption at 77 K). [b] Based on CHN element analysis. [c] g-C_3N_4 was synthesized following the procedure reported by Thomas et al.[7]

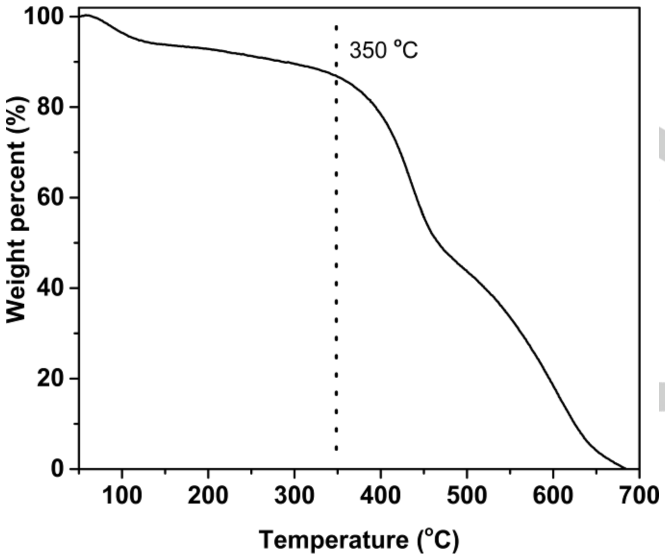

Figure S4. Thermogravimetric curve of MelonHP polymer.

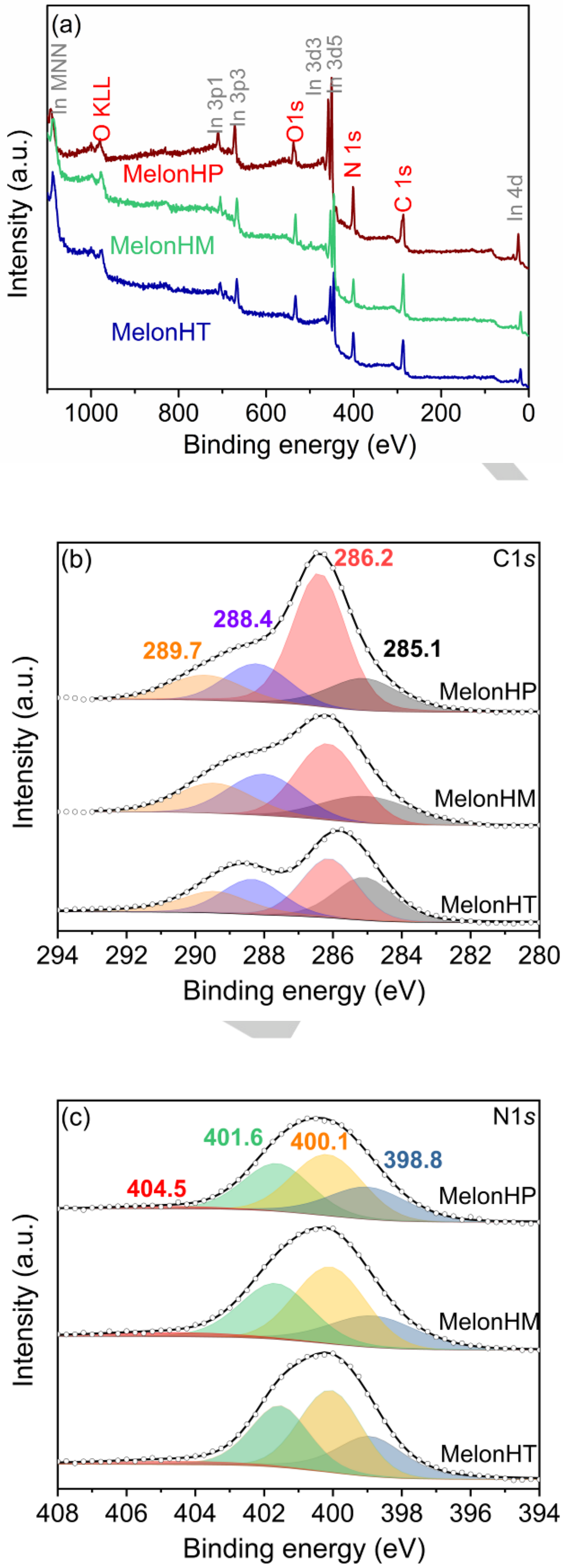

Figure S5. XPS spectra of hydrazone linked heptazine-based porous conjugated polymers: (a) the full survey spectra, (b) high-resolution C1*s* spectra and (c) high-resolution N 1*s* spectra.

Synthesis of MelonB

A flame dried Schlenk flask fitted with a condenser and a magnetic stirring bar was charged with Melem-NH_2 (489 mg, 1.86 mmol), benzaldehyde (356 mg, 3.35 mmol) and DMSO (10 mL). After degassing by argon bubbling the mixture was heated to 120 °C for 120 h under an inert atmosphere. The reaction mixture was cooled to room temperature and poured into cold water. The precipitate was collected by centrifugation, washed with water and methanol for several times, and dried under vacuum to afford model compound. ^{1}H NMR (600 MHz, DMSO-d6): δ (ppm) 8.15 (d, J = 7.8 Hz, 4H), 7.85-7.74 (m, 12H), 7.57 (d, J = 8.2 Hz, 4H), 7.46 (t, J = 7.7 Hz, 4H), 7.35 (t, J = 7.4 Hz, 4H).

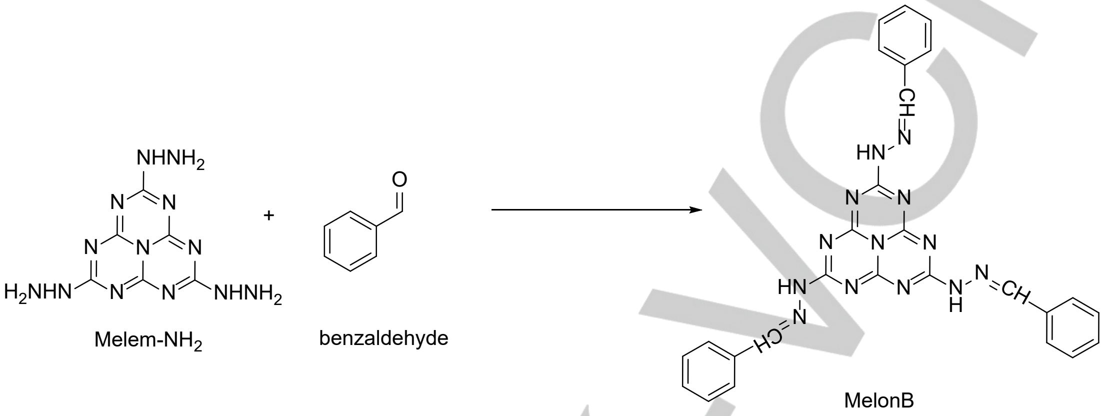

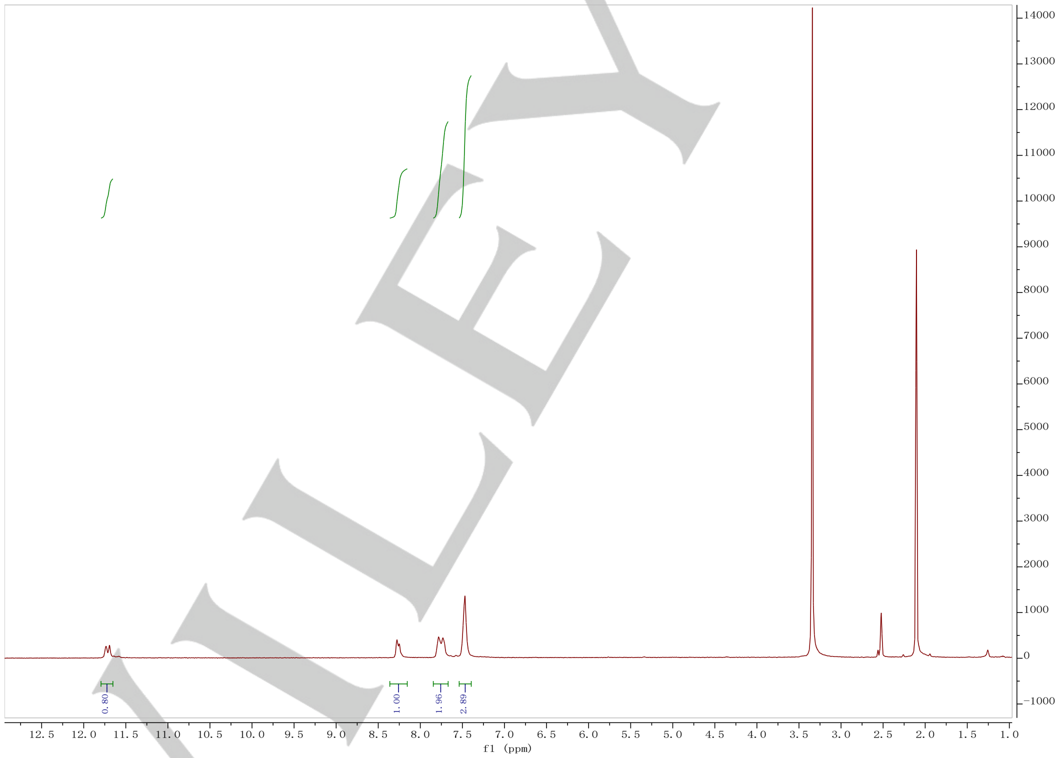

Figure S6. ^{1}HNMR spectrum of melonB in DMSO-d6.

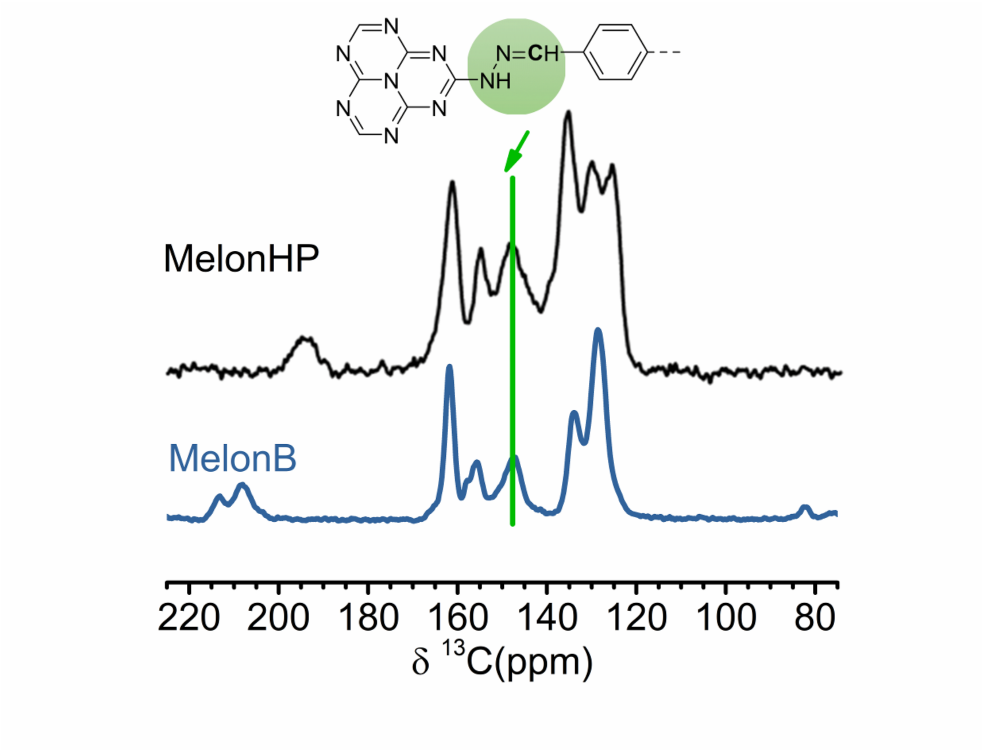

Figure S7. ^{13}C CPMAS SSNMR spectra of MelonB and melonHP.

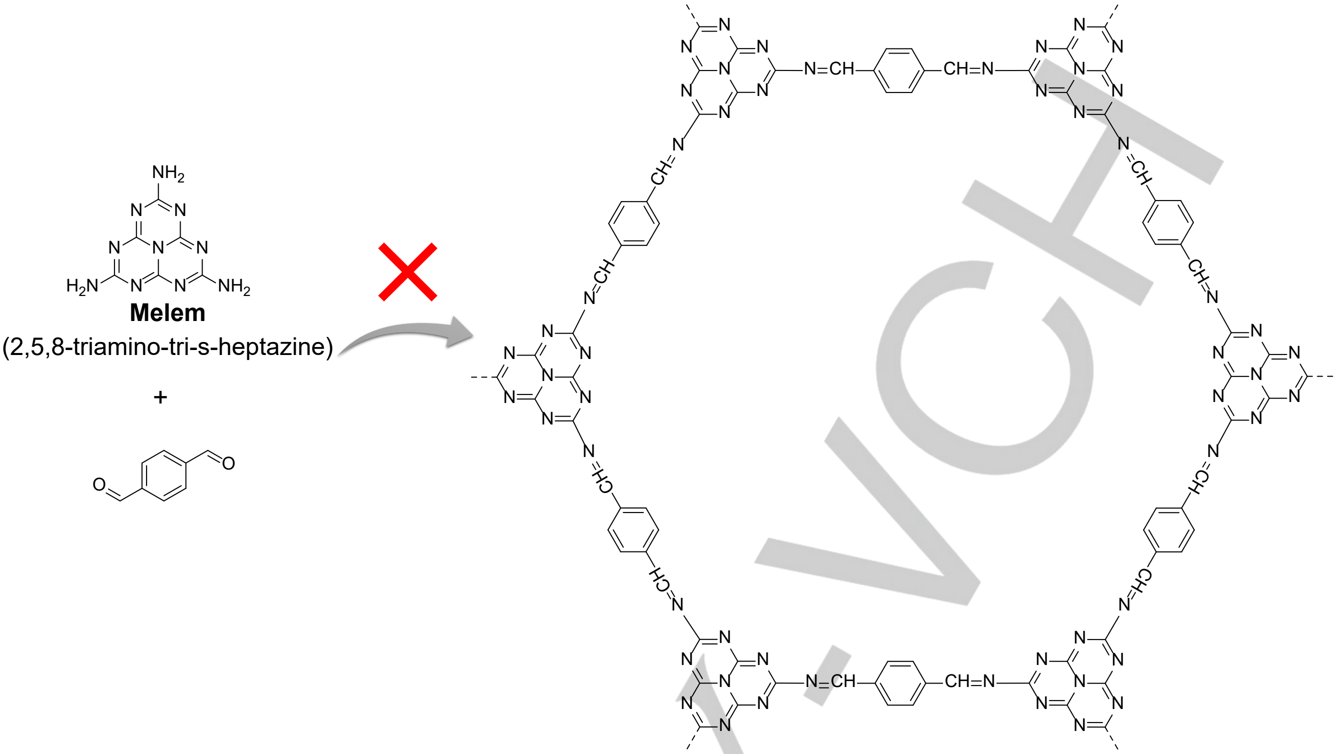

Scheme S1. Schematic illustration of the synthesis off melem-based solid using melem as precursor instead of melem-NH$_2$. Note that the resulting melem-based solid is not hydrazone-linked heptazine-based conjugated polymer (See below, Figure S8 and S9). Melem cannot react with aldehyde due to the electron-deficient heptazine ring that makes the –NH$_2$ groups inert to electrophilic attack

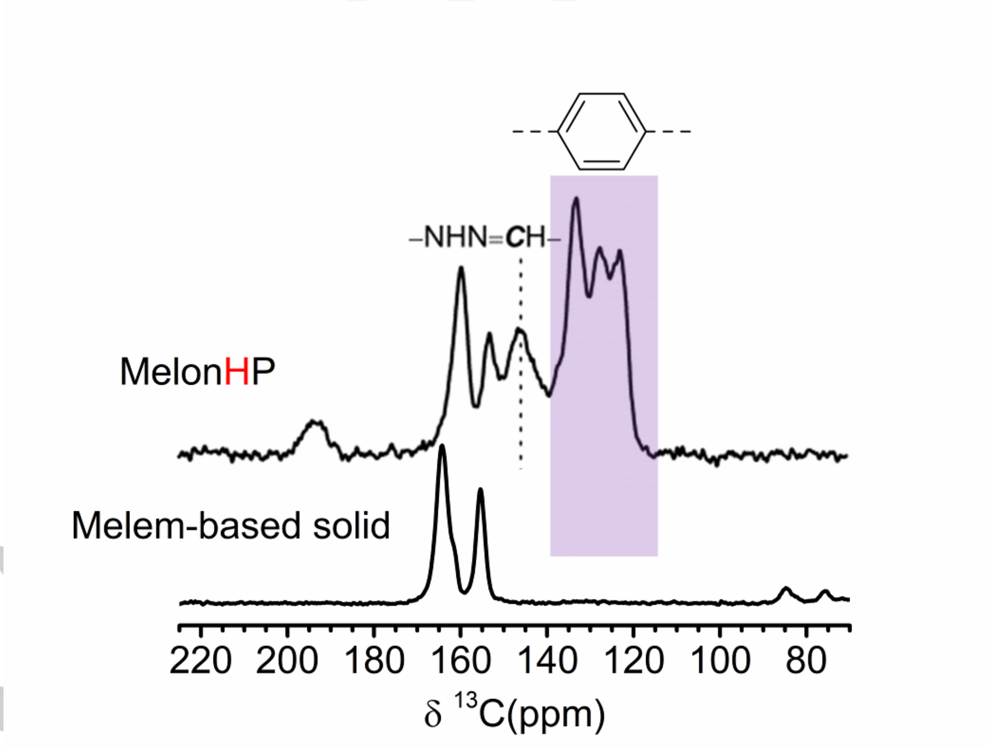

Figure S8. ^{13}C CPMAS SSNMR spectra of melem-based solid and MelonHP.

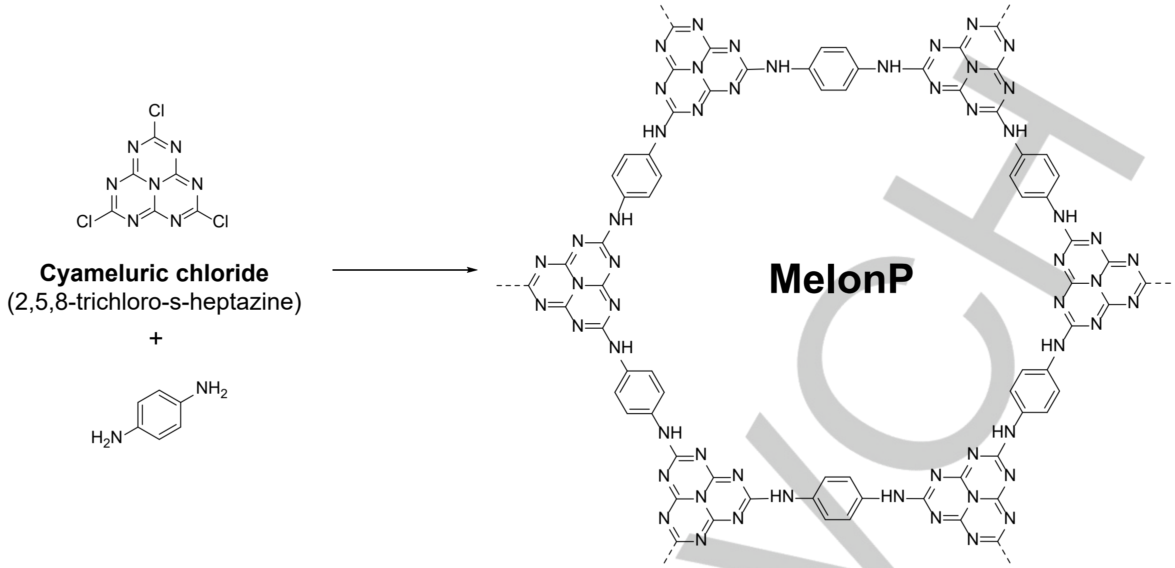

Scheme S2. Schematic illustration of the synthesis of hydrazine-free heptazine-based conjugated polymer using cyameluric chloride and *p*-phenylenediamine as precursors.

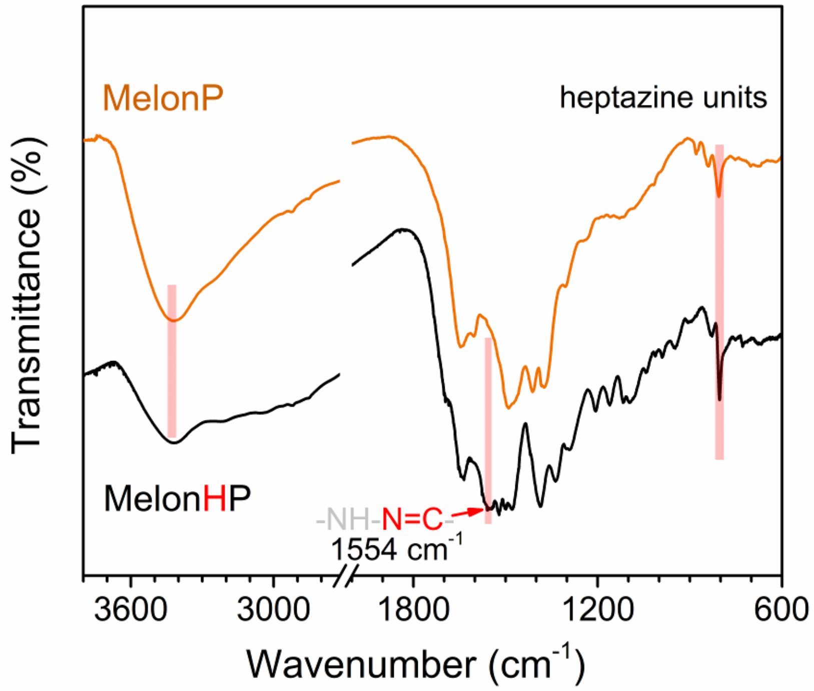

Figure S9. FTIR spectra of heptazine-based MelonP (without hydrazone groups) and MelonHP polymers.

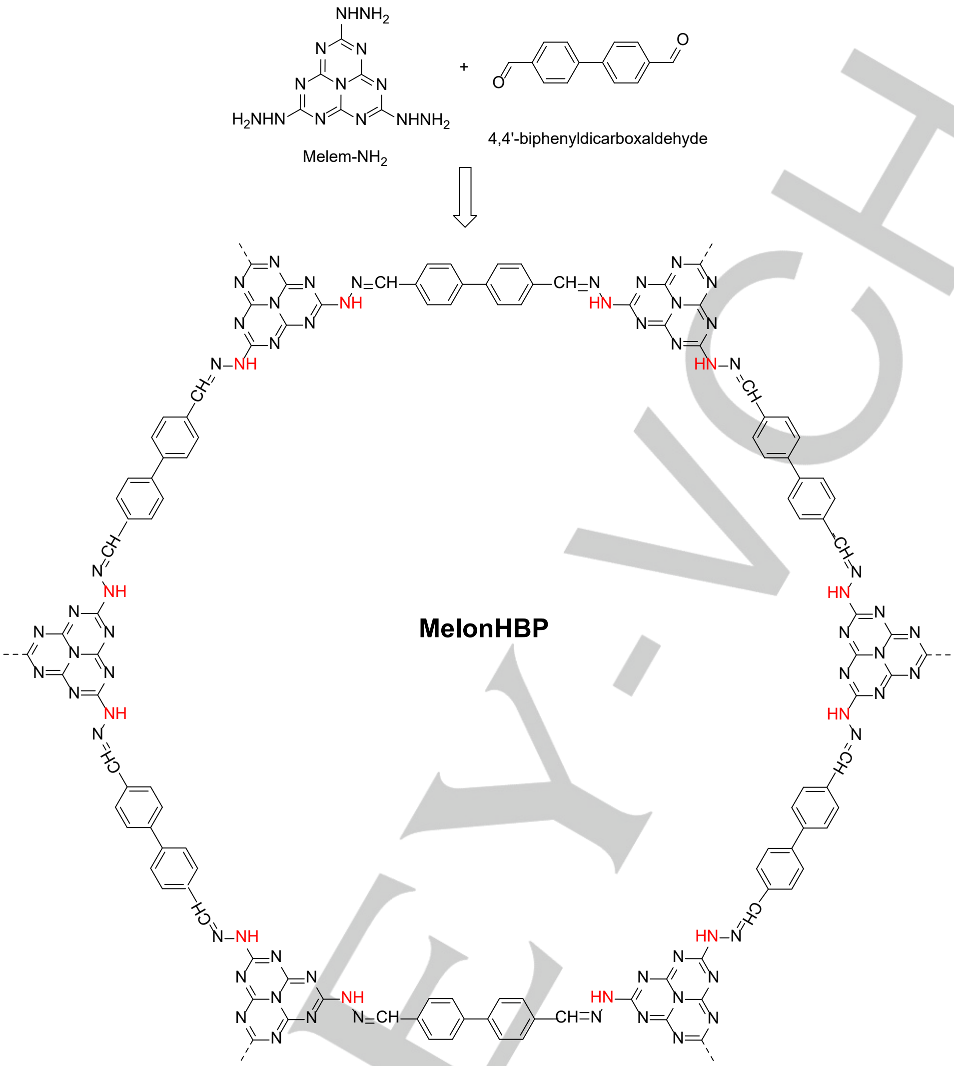

Scheme S3. Schematic illustration of the synthesis of a new control model of heptazine-based polymer via the same method while using 4,4'-biphenyldicarboxaldehyde as the aldehyde precursor (denoted as MelonHBP).

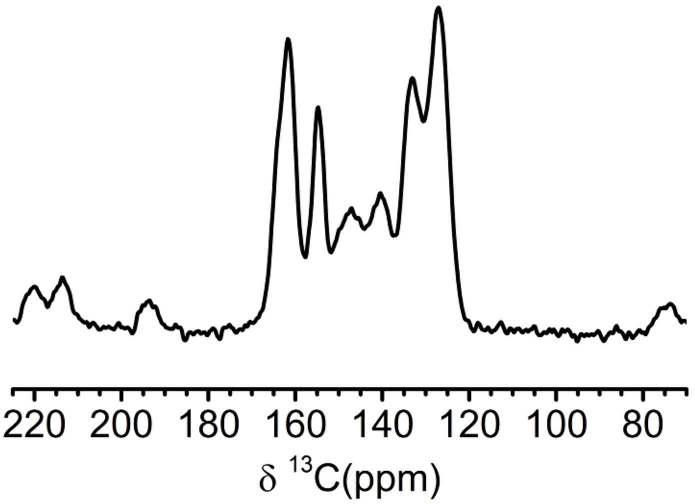

Figure S10. ^{13}C CPMAS SSNMR spectra of MelonHBP.

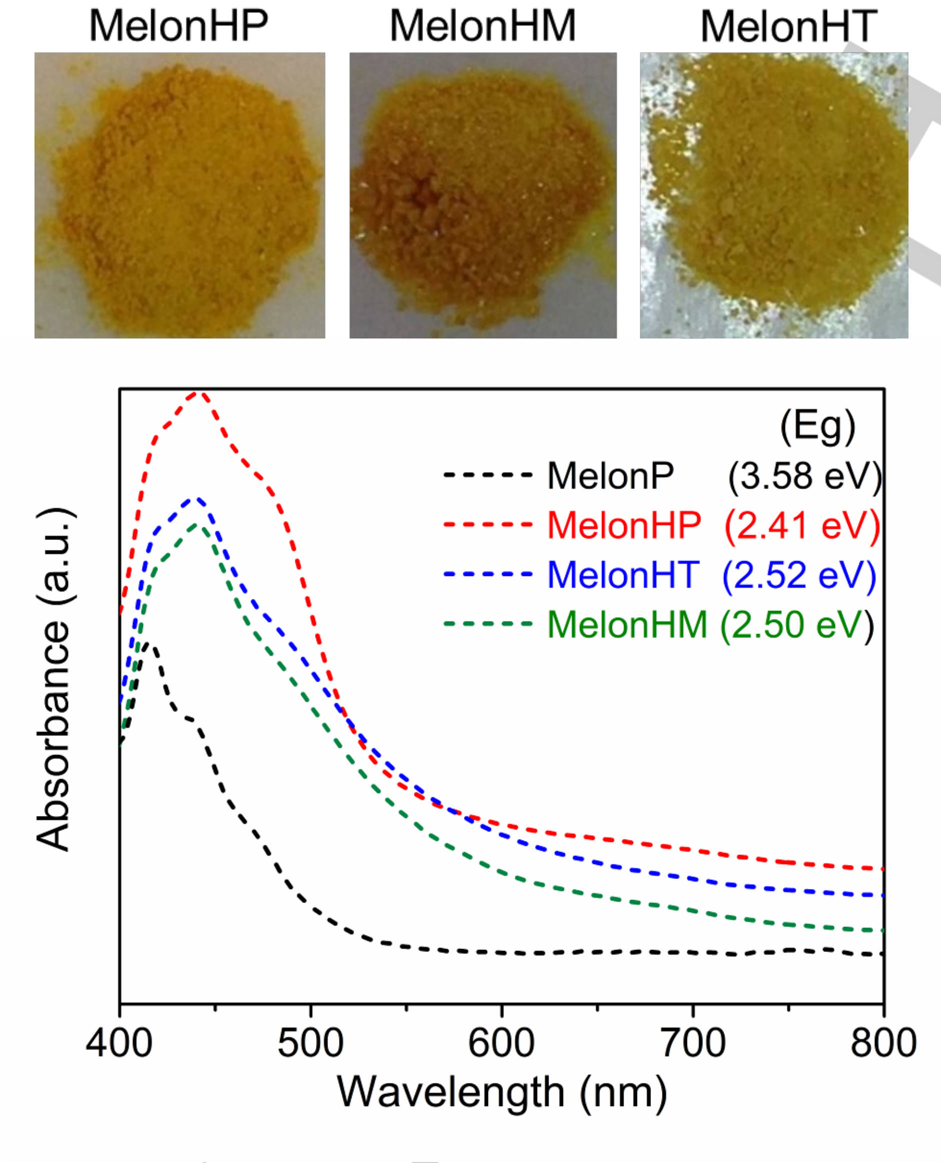

Figure S11. Digital photos and UV-vis absorption spectra of MelonP, MelonHP, MelonHM, and MelonHT, the insets show the corresponding bandgap energy.

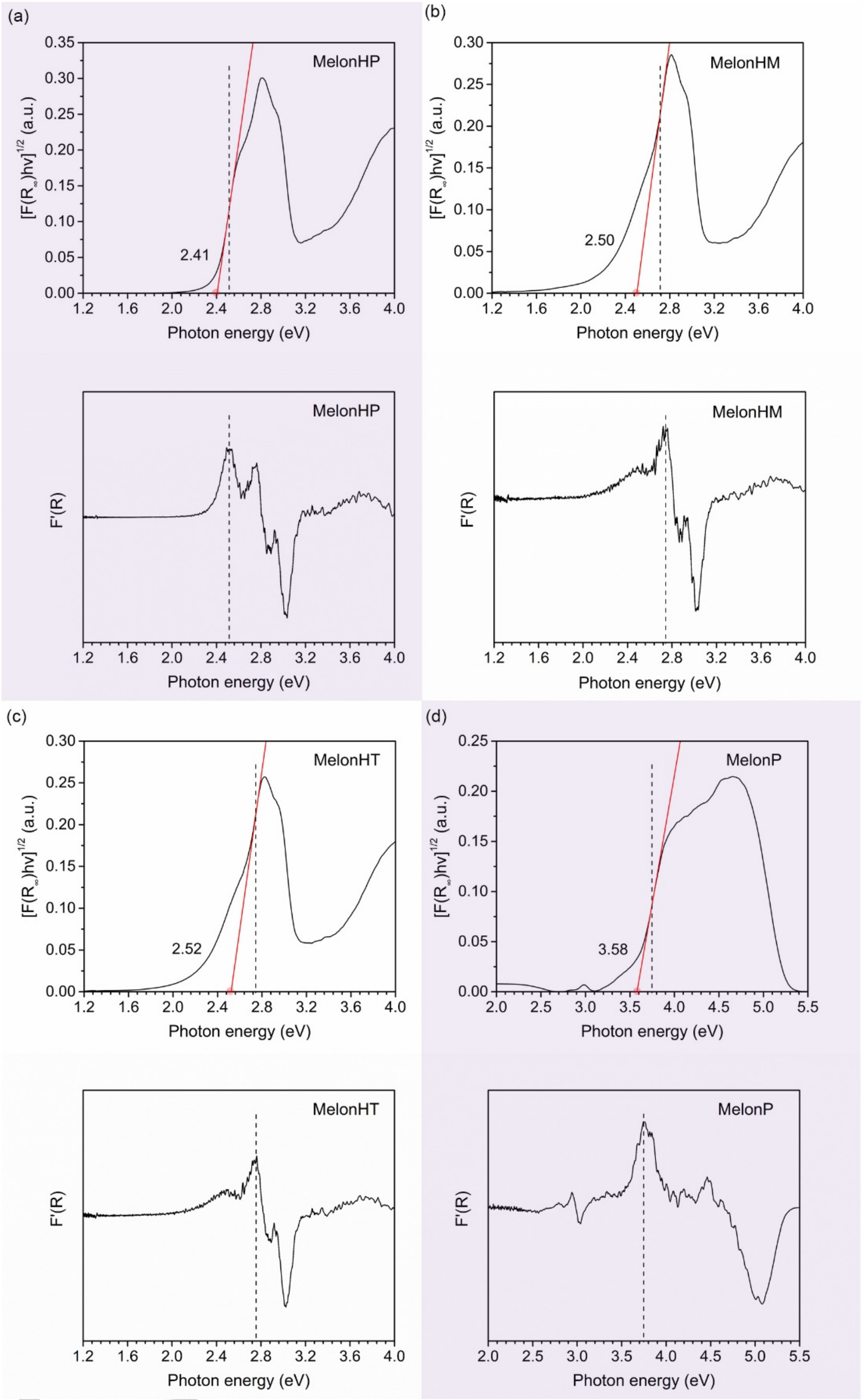

Figure S12. $[F(R_\infty)hv]^{1/2}$ plotted against the photon energy for the determination of bandgap energy (E_g) for MelonHP (a), MelonHM (b), MelonHT (c) and MelonP (d). The E_g value is determined by finding the intercept on the X-axis of the tangent line in the low-energy rise of the plot of $[F(R_\infty)hv]^{1/2}$ vs. hv.

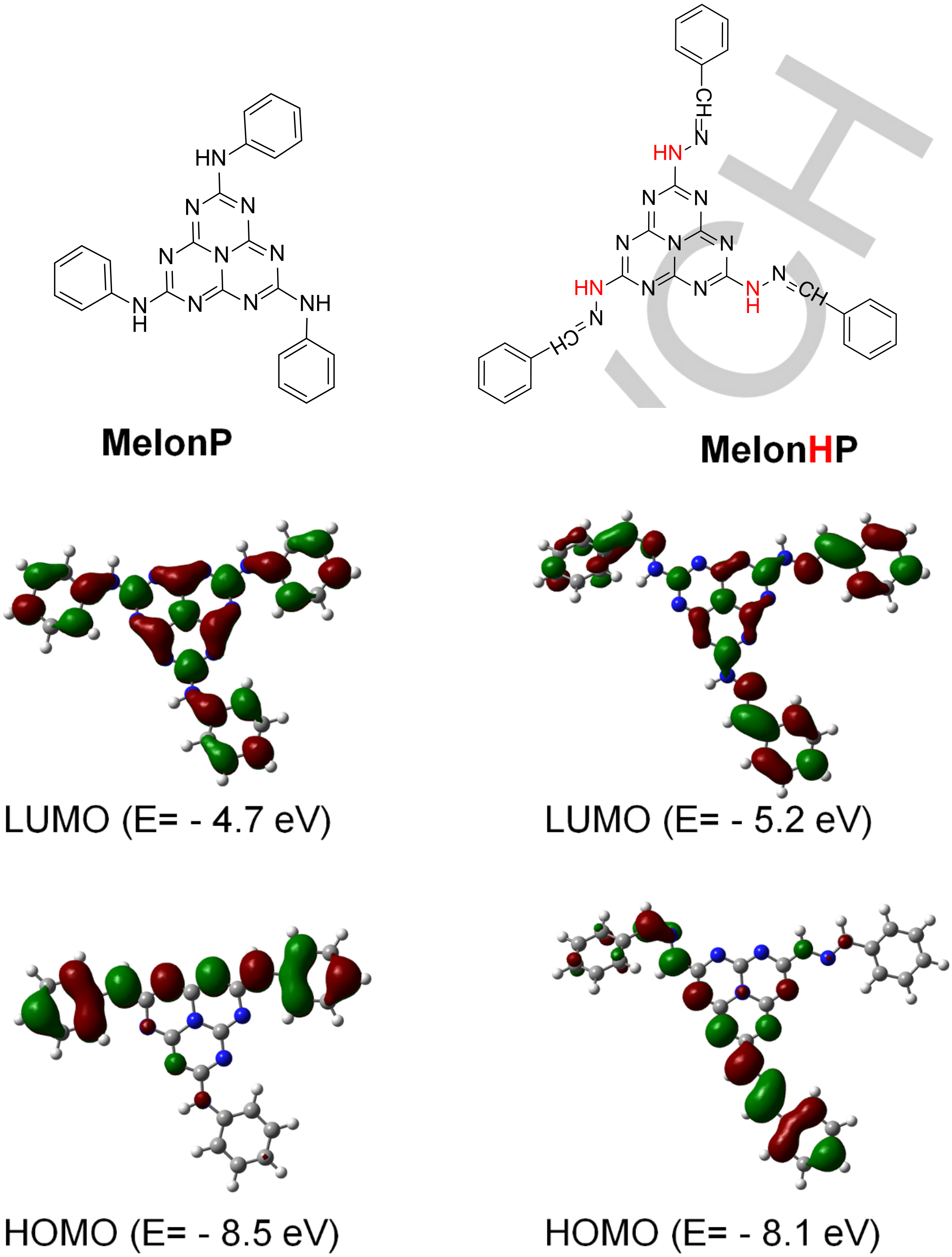

Figure S13. Representative structure of the repeating units in the MelonP and MelonHP, and the corresponding theoretical HOMO and LUMO levels via CP2K, respectively.

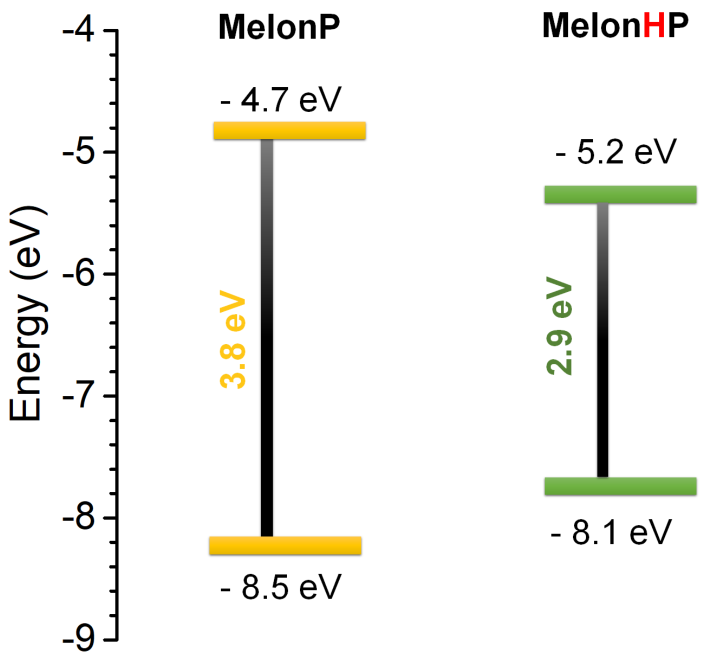

Figure S14. Band energy diagram of MelonP and MelonHP.

References

[1] T. Saplinova, V. Bakumov, T. Gmeiner, J. Wagler, M. Schwarz and E. Kroke, Z. *Anorg. Allg. Chem*., **2009**, *635*, 2480.

[2] Y. Ishii and R. Tycko, *J. Magn. Reson.*, **2000**, *142*, 199.

[3] T. Kobayashi, Y. Nishiyama and M. Pruski, in *Modern Methods in Solid-state NMR: A Practitioner's Guide*, The Royal Society of Chemistry, **2018**, DOI: 10.1039/9781788010467-00001, pp. 1.

[4] J. Hutter, M. Iannuzzi, F. Schiffmann and J. VandeVondele, Wiley Interdiscip. *Rev. Comput. Mol. Sci.*, **2014**, *4*, 15.

[5] J. VandeVondele, M. Krack, F. Mohamed, M. Parrinello, T. Chassaing and J. Hutter, *Comput. Phys. Commun.*, **2005**, *167*, 103.

[6] S. Grimme, J. Antony, S. Ehrlich and H. Krieg, *J. Chem. Phys.*, **2010**, *132*, 154104.

[7] F. Goettmann, A. Fischer, M. Antonietti, A. Thomas, *Angew. Chem. Int. Ed.* **2006**, 45, 4467.

[8] B. Jürgens, E. Irran, J. Senker, P. Kroll, H. Müller, W. Schnick, *J. Am. Chem. Soc.* **2003**, *125*, 10288.